

## Supporting Information

### Surface-anchoring fluorinated sulfonate enables efficient and stable perovskite photovoltaics

Bo Yang,<sup>ab</sup> Xinyue Li,<sup>c</sup> Bing Cai,\*<sup>c</sup> Xiaojia Zheng,<sup>ab</sup> Kai Xiong\*<sup>c</sup> and Wen-Hua Zhang\*<sup>c</sup>

<sup>a</sup> Institute of Chemical Materials, China Academy of Engineering Physics, Mianyang 621900, China.

<sup>b</sup> National Energy Novel Materials Center, Chengdu 610200, China.

<sup>c</sup> Yunnan Key Laboratory of Carbon Neutrality and Green Low-carbon Technologies, School of Materials and Energy, Yunnan University, Kunming 650000, China.

E-mail addresses: bingcai@ynu.edu.cn (B. Cai), xiongkai@ynu.edu.cn (K. Xiong), wenhua.zhang@ynu.edu.cn (W.-H Zhang)

## Experimental Section

**Materials:** Lead iodide ( $\text{PbI}_2$ ) was obtained from Advanced Election Technology Co., Ltd. Methylammonium iodide (MAI), methylammonium chloride (MACl), formamidinium iodide (FAI), poly(triaryl amine) (PTAA) and 2,2',7,7'-tetrakis[N,N-di(4-methoxyphenyl)amino]-9,9'-spirobifluorene (Spiro-OMeTAD) were bought from Xi'an Yuri Solar Co., Ltd. Cobalt (III) tris(bis(trifluoromethylsulfonyl)imide) salt (Co(III)TFSI, FK209) and 4-isopropyl-4'-methyl diphenyliodonium tetrakis(pentafluorophenyl)borate (TFPB) were purchased from Greatcell solar and TCI, respectively. 4-tert-butylpyridine (4-tBP) and lithium bis(trifluoromethanesulfonyl)imide salt (Li-TFSI) were bought from Sigma-Aldrich. The dimethyl sulfoxide (DMSO), N, N-dimethylformamide (DMF), acetonitrile (ACN) chlorobenzene (CB), isopropyl alcohol (IPA), and diphenyl-(trifluoromethyl)-sulfonium trifluoromethanesulfonate (TFS-TFMS) were purchased from Aladdin. Glass substrates of indium doped tin oxide (ITO) were gained from South China Science and Technology Co., Ltd.

**Devices fabrication:** The glass/ITO substrates were sequentially washed by detergent (40 min), deionized water (30 min) and ethanol (60 min) under sonication. Moreover, these substrates were treated with ultraviolet-ozone for 40 min in air environment. The  $\text{SnO}_2$  nanocrystals/ethanol solution ( $\sim 12 \text{ mg mL}^{-1}$ ) was spin-coated (3000 rpm for 30s) onto the above substrates to form as-prepared  $\text{SnO}_2$  films, which were then annealed at 150 °C for 30 min and ultraviolet-ozone for 20 min, sequentially.  $\text{SnO}_2$  nanocrystals were synthesized by referring to our previous work.<sup>1</sup> 691.5 mg of  $\text{PbI}_2$  was dissolved into a co-solvent (900  $\mu\text{L}$  of DMF:100  $\mu\text{L}$  of DMSO) under stirring 1 h at 60 °C.  $\text{PbI}_2$  solution (30  $\mu\text{L}$ ) was dropped onto the center of a  $\text{SnO}_2$  film and spin-coated at 1550 rpm for 40 s. And the light-yellow film was annealed at 70 °C (70~90 s) in a  $\text{N}_2$ -fulled glovebox (24~26 °C). Next, an as-prepared perovskite film was initially formed by quickly dropping 60  $\mu\text{L}$  organic solution onto the  $\text{PbI}_2$  films that was made up of FAI (90 mg), MACl (9 mg), and MAI (6.4 mg) in 1 mL IPA, where the parameter for spin-coating was 2000 rpm for 30 s. Importantly, the as-prepared films were further annealed at 150 °C (15 min) under air with 30~40% relative humidity to gain photo-active phase absorbers, which were immediately transferred into a  $\text{N}_2$ -fulled glovebox after finishing anneal process. For the TFS-TFMS modified devices, 50  $\mu\text{L}$  of TFS-TFMS/IPA solution ( $0.5\text{--}3.0 \text{ mg mL}^{-1}$ ) was dynamically dropped onto perovskite films at 5000 rpm (30 s) and the obtained film was annealed at 100 °C (10 min). To fabricating a complete device, 30  $\mu\text{L}$  of spiro-OMeTAD/CB ( $101.2 \text{ mg mL}^{-1}$ ) solution was deposited onto control or modified films at 4500 rpm (30 s) without annealing, where the additives consisted of 24.5  $\mu\text{L}$  Li-TFSI/ACN ( $520 \text{ mg mL}^{-1}$ ), 49  $\mu\text{L}$  FK209/ACN ( $300 \text{ mg mL}^{-1}$ ) and 40  $\mu\text{L}$  4-

tBP. The PTAA with good thermostability was adopted as a hole-transportation-layer to evaluate thermal aging capacity (85 °C) for PSCs. Finally, gold electrodes were thermally evaporated on the above films with a metal shadow mask of 0.09 cm<sup>2</sup>.

**Characterizations:** The morphologies characteristics of films were observed by field emission scanning electron microscopy (FESEM) and atomic force microscopy (AFM), respectively. The crystal structure of perovskite films was characterized on a D8 X-ray diffractometer (XRD). The compositional depth analysis for semi-complete devices was recorded by time-of-flight secondary-ion mass spectrometry (IONTOF TOF-SIMS5) with negative polarity. The chemical interaction between TFS-TFMS and perovskites was measured by Raman microscope with an excitation wavelength of 532 nm (Renishaw inVia), Liquid state nuclear magnetic resonance (JNM-ECZ400S/L1), X-ray photoelectron spectroscopy (Thermo-Fisher ESCALAB Xi<sup>+</sup> system), and Fourier transform infrared spectrometer under a transmission mode (Thermo Scientific Nicolet iS5). The detailed test process of FTIR was as following: (1) A mixed powder with TFS-TFMS and PbI<sub>2</sub> or FAI (mass ratio 1:3) was evenly grind about 5 min and then was annealed on a hotplate at 100 °C for 10 min. Similarly, for the perovskite/TFS-TFMS sample, the perovskite film was first deposited on the glass substrate and then was scraped off to blend with TFS-TFMS according to the above fabricated process. The pure sample was also processed as the above method before testing. (2) The test range was set from 4000 to 600 cm<sup>-1</sup> and the scanning times was chosen as 32. Before samples testing, the background should be token out by testing the blank. The surface contact potential difference (CPD) of films was acquired *via* Kelvin probe force microscopy (Bruker Dimension). The steady-state and time-resolved photoluminescence (PL/TRPL) spectra were performed by a FLS1000 Series of Fluorescence Spectrometers in air atmosphere at room temperature. The laser with a wavelength of 485 nm was employed as an excitation light source, which was incident on the surface of perovskite films. A QE-R3011 testing system (Enlitech) was served as recording external quantum efficiency (EQE) spectra of devices. A multi-channel electrochemical workstation (VMP3, Biologic) was utilized as collecting mott-schottky (M-S) curves and electrochemical impedance spectroscopy (EIS) with a frequency range from 1 MHz to 100 mHz for PSCs. In a N<sub>2</sub>-filled glovebox at RT, the current-voltage curves of PSCs were performed by a Keithley digital source meter (Model 2400) and a Xenon lamp solar simulator with standard AM 1.5G (100 mW·cm<sup>-2</sup>, SSF5-3A, Enlitech) that was calibrated by a silicon cell. The *J-V* curves for devices with a test area of 0.09 cm<sup>2</sup> were collected under two sweep modes of forward scan (from -0.1 to 1.2 V) and reverse scan (from 1.2 to -0.1 V).

**Theoretical calculation:** The electrostatic potential (ESP) of TFS-TFMS was calculated by using the DMol<sup>3</sup> code. The electron interactions were explored by Perdew-Burke-Ernzerhof (PBE) exchange-correlation function within the generalized gradient approximation (GGA).<sup>2-</sup><sup>3</sup> The double numerical polarization (DNP) function basis set was selected to expand the molecular orbitals, whose cutoff was chosen to be 4.4 Å. All electrons were employed to treat the core electrons. The geometry optimization convergence thresholds between optimization cycles, including maximum force, energy change, and maximum displacement were set to be 0.004 hartree/Å, 10<sup>-5</sup> hartree, and 0.005 Å, respectively. The 10<sup>-6</sup> hartree was adopted as the electronic self-consistent field convergence threshold. The smearing parameter of 0.005 hartree during thermal smearing was applied to the orbital occupation to speed up the convergence.

The energy and charge density difference (CDD) computations were carried out using the Cambridge Sequential Total Energy Package (CASTEP), which was on the foundation of the pseudopotential plane wave (PPW) method.<sup>4</sup> The ultrasoft (USP) potentials was utilized as describing electron-ion interactions. Expanding the wave functions with a cutoff kinetic energy of 480 eV was gained when a plane-wave basis set was used. The function parametrized by PBE, that is a form of the general gradient approximation (GGA), was throughout adopted for the electron-electron exchange and correlation interactions. In this work, the Monkhorst-Pack (MP) grids of special points with the separation of 0.08 Å<sup>-1</sup> was served for Brillouin-zone integrations.

The 2×2×2 FAPbI<sub>3</sub> supercell was constructed. All adsorptive binding energies ( $E_{ads}$ ) between perovskites and TFMS<sup>-</sup> used in this work were defined as:

$$E_{ads} = E_{total} - (E_{slab} + E_{adsorbate})$$

The  $E_{total}$  presented the total energy of the adsorbate and slab interacting system. The  $E_{adsorbate}$  and  $E_{slab}$  can be responsible for energies of the isolated adsorbate and the slab of a supercell, respectively.

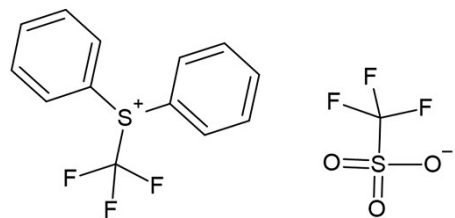


**Fig. S1** The chemical structure of the TFS-TFMS molecule.

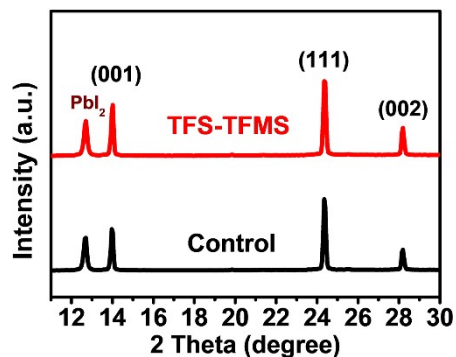


**Fig. S2** The XRD pattern of the control and TFS-TFMS optimized perovskite films.

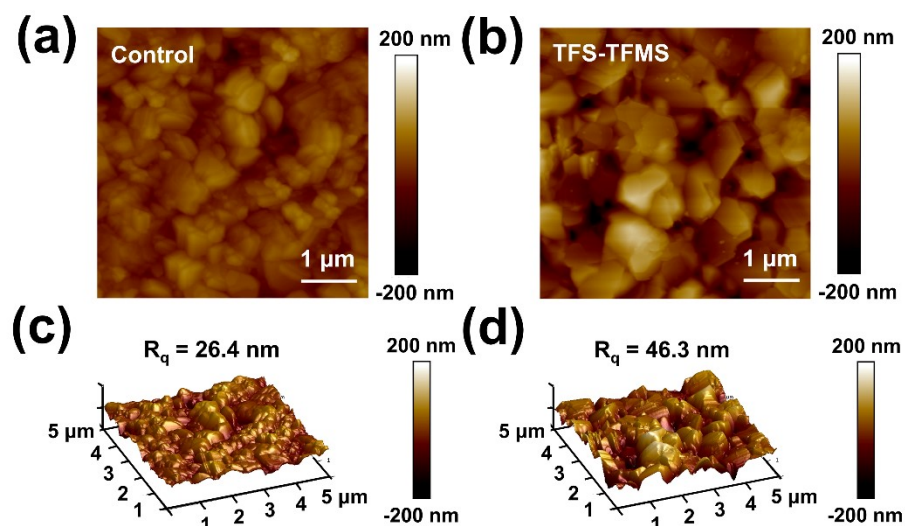


**Fig. S3** AFM images and the corresponding 3D maps of the (a, c) control and (b, d) TFS-TFMS optimized perovskite films.

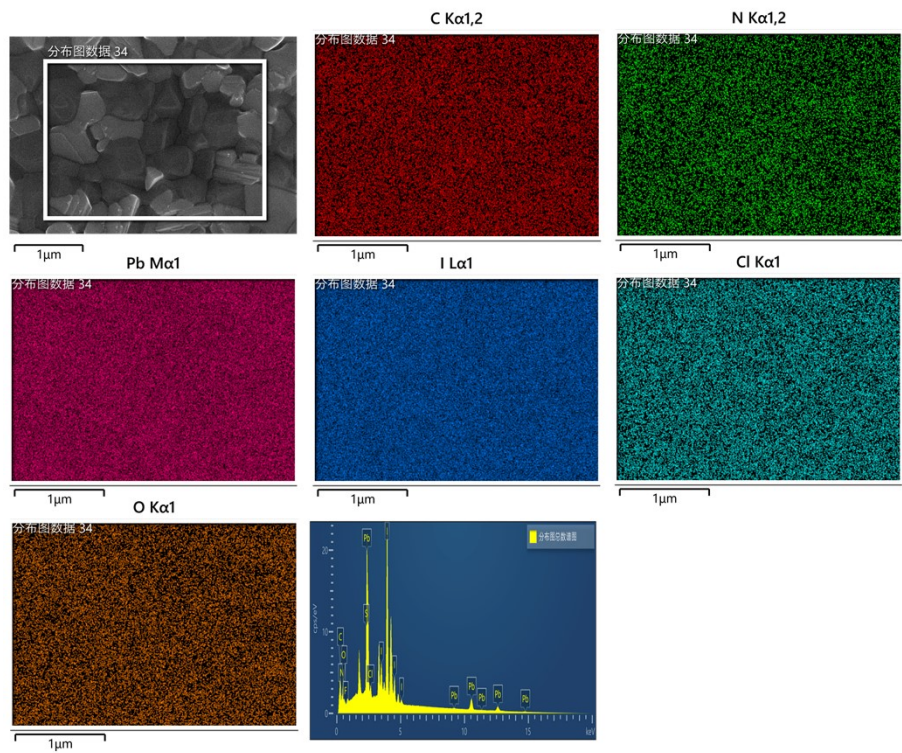


**Fig. S4** EDS mapping of the control perovskite film.

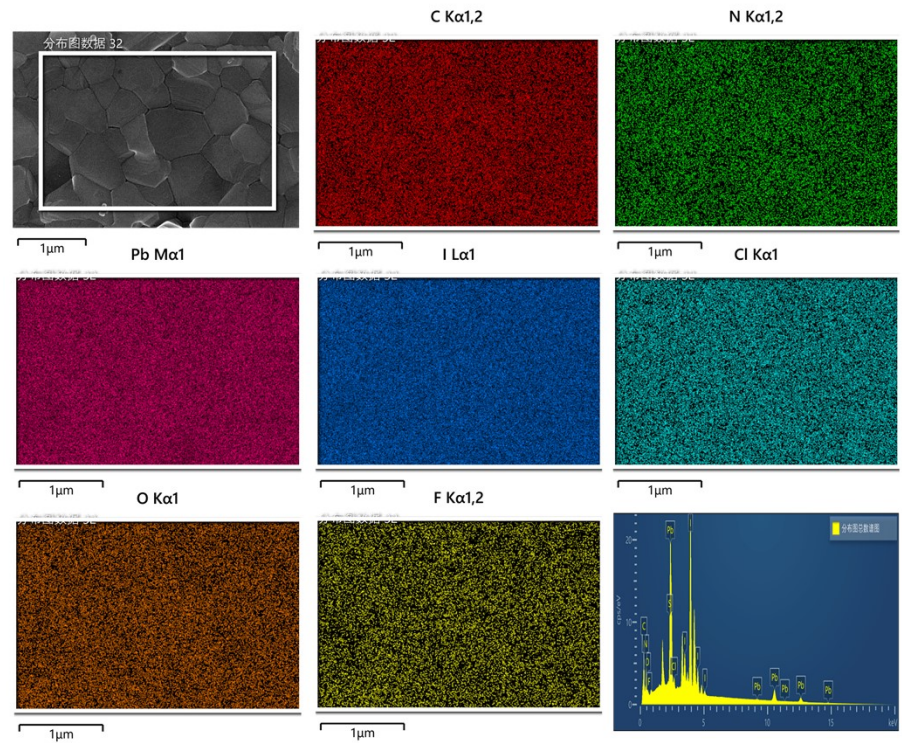


**Fig. S5** EDS mapping of the TFS-TFMS optimized perovskite film.

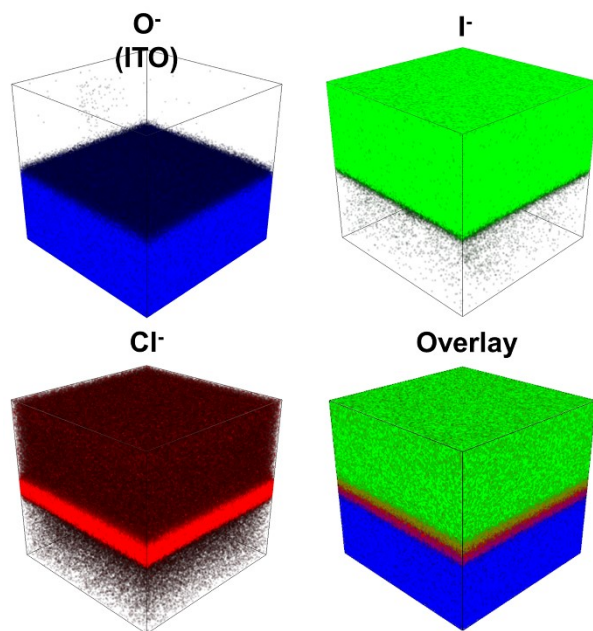


**Fig. S6** Reconstructed 3D maps of negative ions for the control perovskite film.

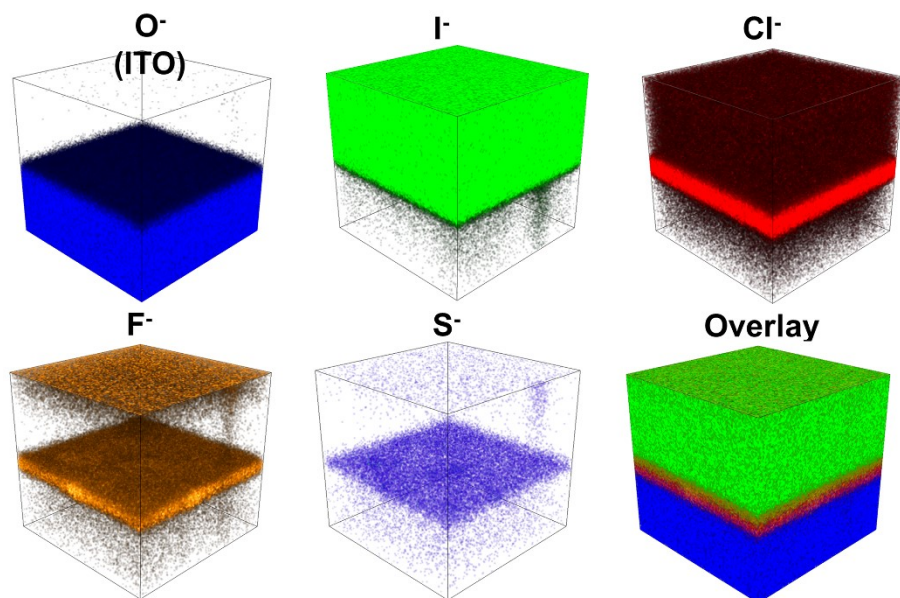


**Fig. S7** Reconstructed 3D maps of negative ions for the TFS-TFMS optimized perovskite film.

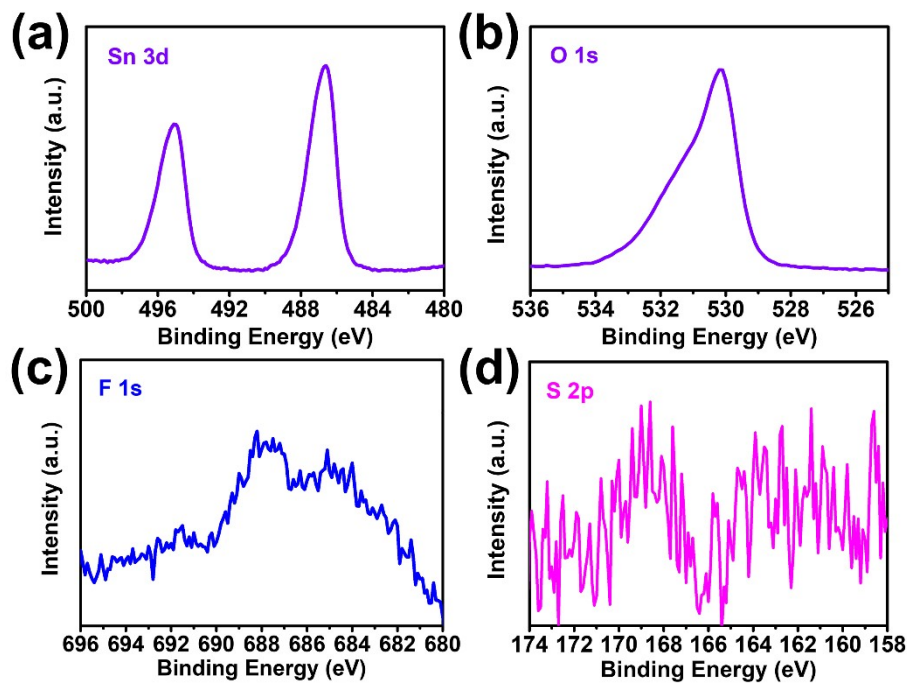


**Fig. S8** High resolution XPS spectra of (a) Sn 3d, (b) O 1s, (c) F 1s, and (d) S 2p for SnO<sub>2</sub> nanocrystal films on glass substrates.

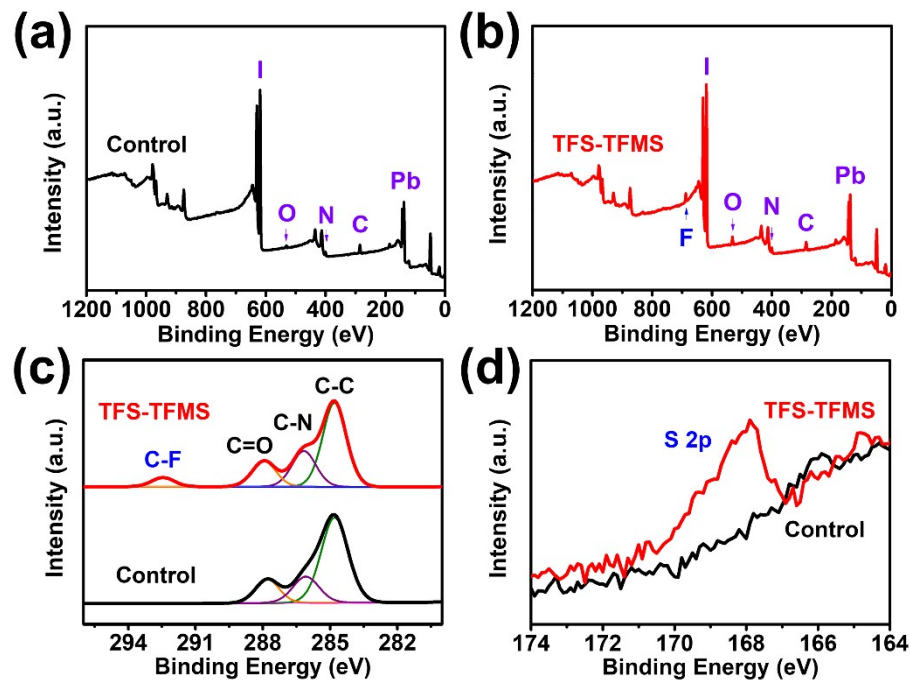


**Fig. S9** XPS spectra of the control and TFS-TFMS optimized perovskite films.

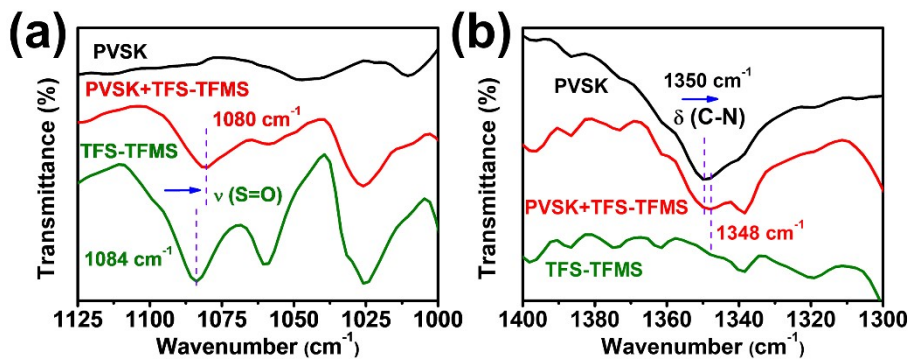


**Fig. S10** FTIR spectra of PVSK, TFS-TFMS and PVSK mixed TFS-TFMS samples.

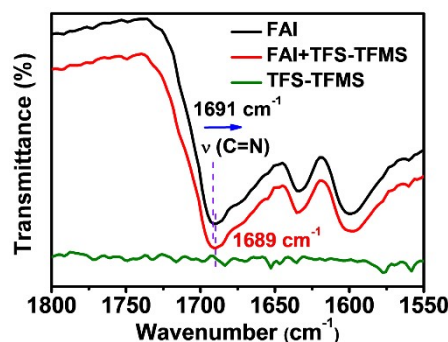


**Fig. S11** FTIR spectra of FAI, TFS-TFMS and FAI blended TFS-TFMS samples.

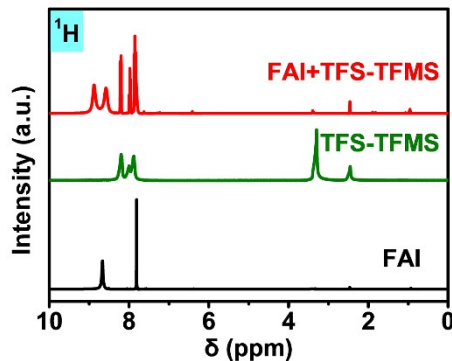


**Fig. S12** <sup>1</sup>H NMR spectra of FAI, TFS-TFMS and FAI/TFS-TFMS mixture.

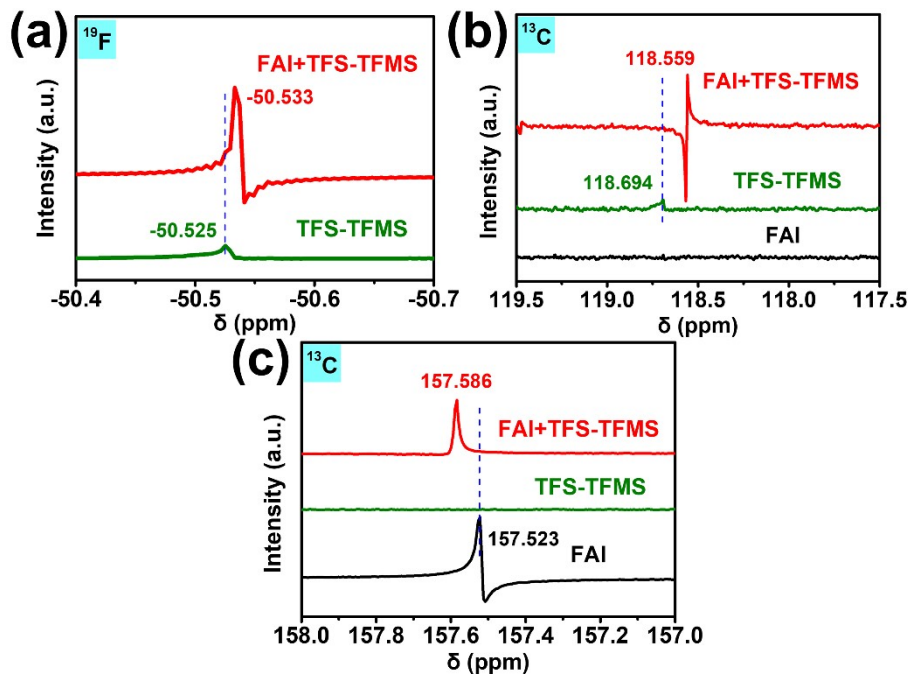


**Fig. S13** (a)  $^{19}\text{F}$  NMR and (b, c)  $^{13}\text{C}$  NMR spectra of FAI, TFS-TFMS and FAI/TFS-TFMS mixture.

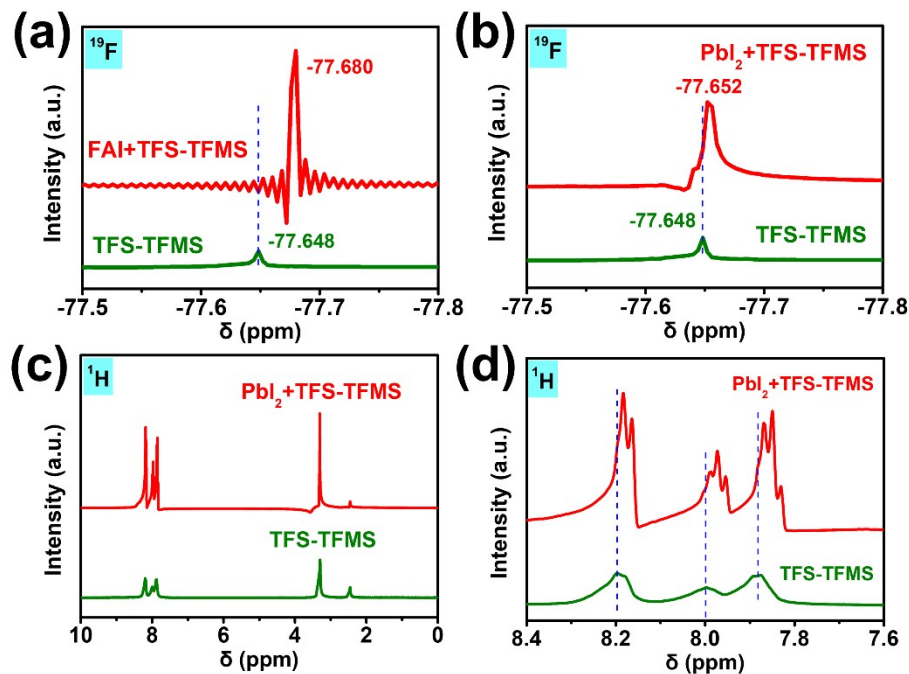


**Fig. S14**  $^{19}\text{F}$  NMR of (a) TFS-TFMS and FAI/TFS-TFMS mixture, (b) TFS-TFMS and  $\text{PbI}_2$ /TFS-TFMS mixture. (c-d)  $^1\text{H}$  NMR of TFS-TFMS and  $\text{PbI}_2$ /TFS-TFMS mixture.

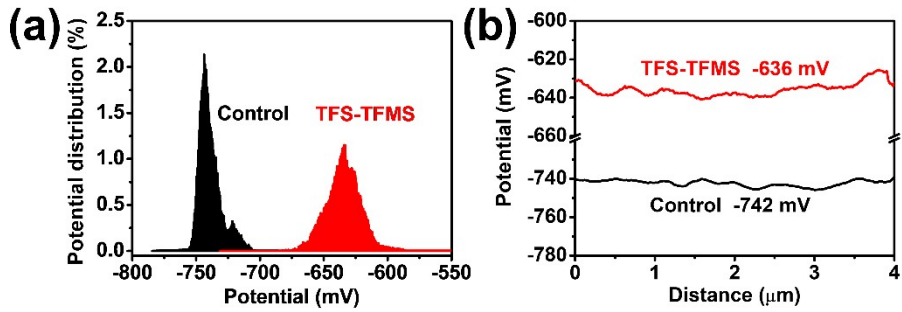


**Fig. S15** (a) The surface contact potential difference (CPD) distributions and (b) the corresponding average values derived from KPFM images for the control and TFS-TFMS optimized films.

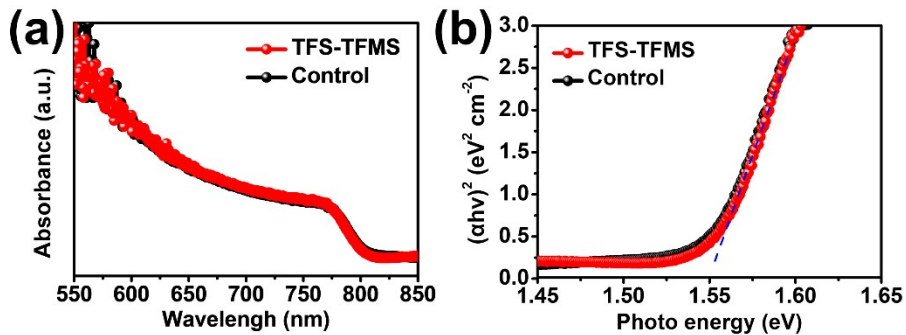


**Fig. S16** (a) UV-vis absorption spectra of the control and TFS-TFMS optimized films. (b) The corresponding bandgaps ( $\sim 1.55$  eV).

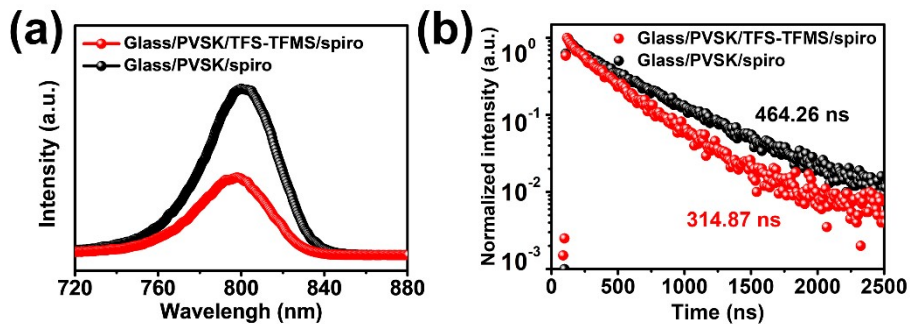


**Fig. S17** (a) PL and (b) TRPL spectra of the control and TFS-TFMS optimized perovskite films employing spiro-OMeTAD as a quenching layer.

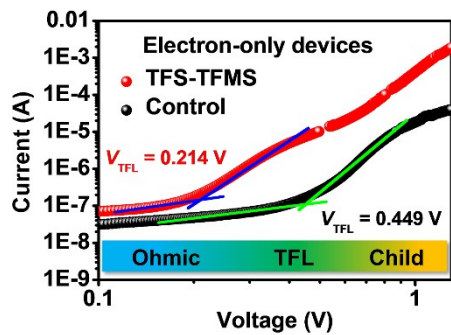


**Fig. S18** Dark  $I$ - $V$  curves of electron-only devices, which was the configuration of ITO/SnO<sub>2</sub>/perovskite/PCBM/BCP/Au, employing TFS-TFMS as a modifier.

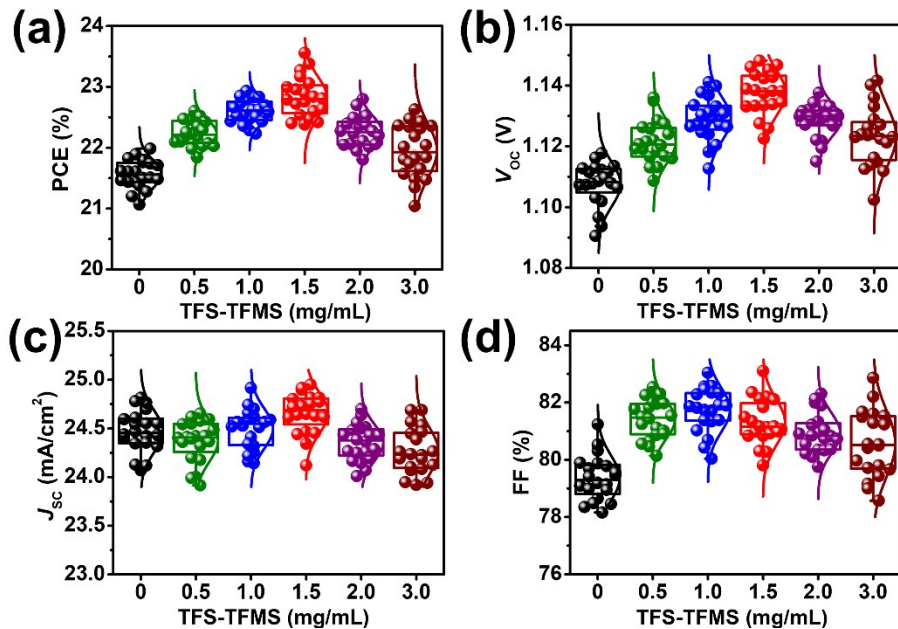


**Fig. S19** Photovoltaic parameter distributions of PSCs adopting different TFS-TFMS concentrations (20 devices for each concentration).

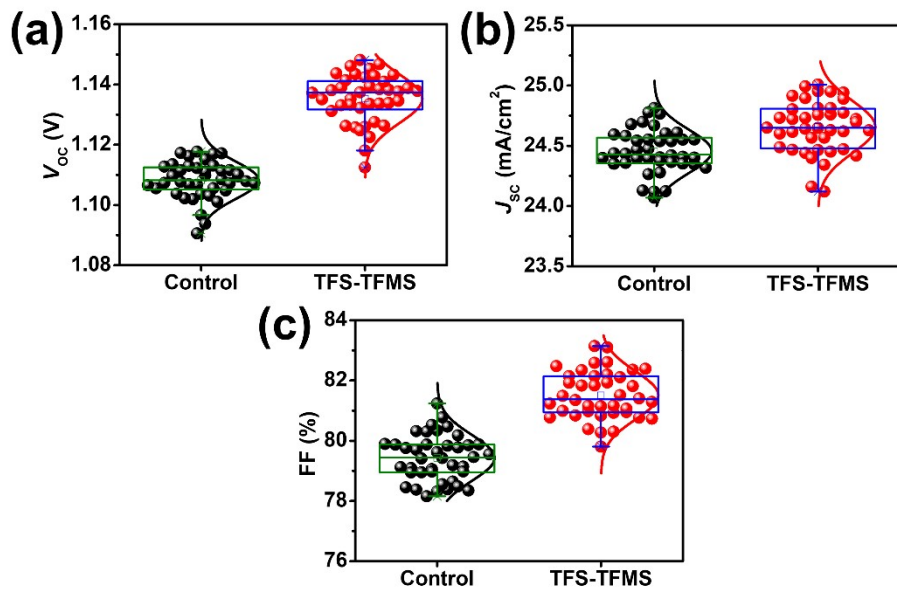


**Fig. S20** Photovoltaic parameter distributions for the control and TFS-TFMS optimized PSCs (40 devices for each condition).

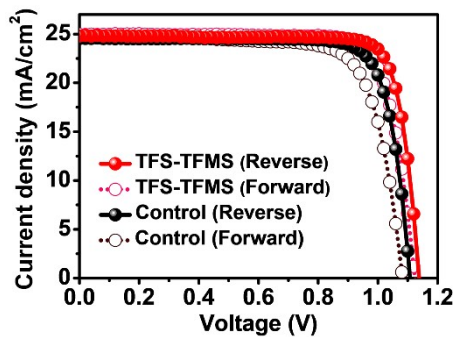


**Fig. S21** The forward and reverse  $J-V$  curves for the control and TFS-TFMS optimized PSCs.

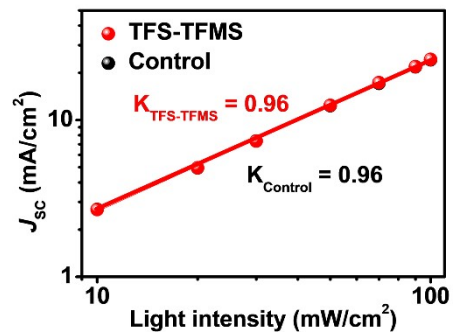


**Fig. S22**  $J_{sc}$  vs. light intensity for PSCs without and with TFS-TFMS modification.

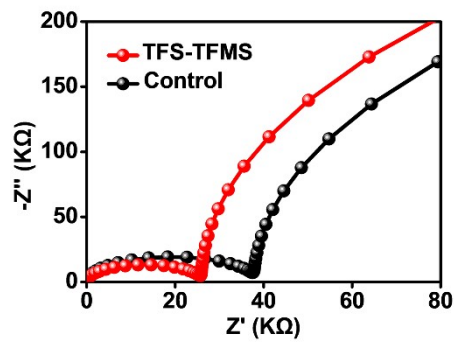


**Fig. S23** Enlarged EIS in high frequency area of Fig. 5i.

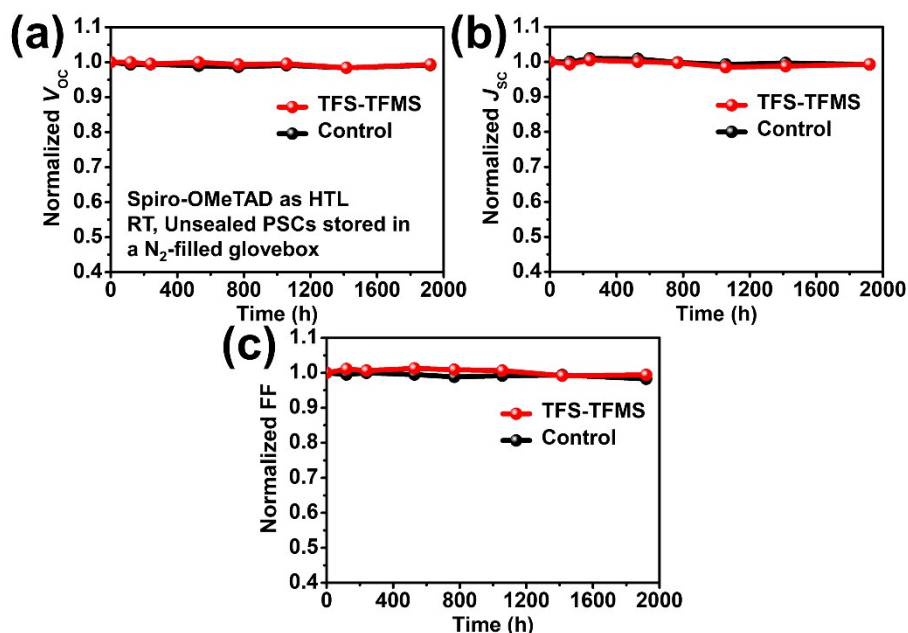


**Fig. S24** RT aging of the unencapsulated PSCs reserved in inert atmosphere under dark.

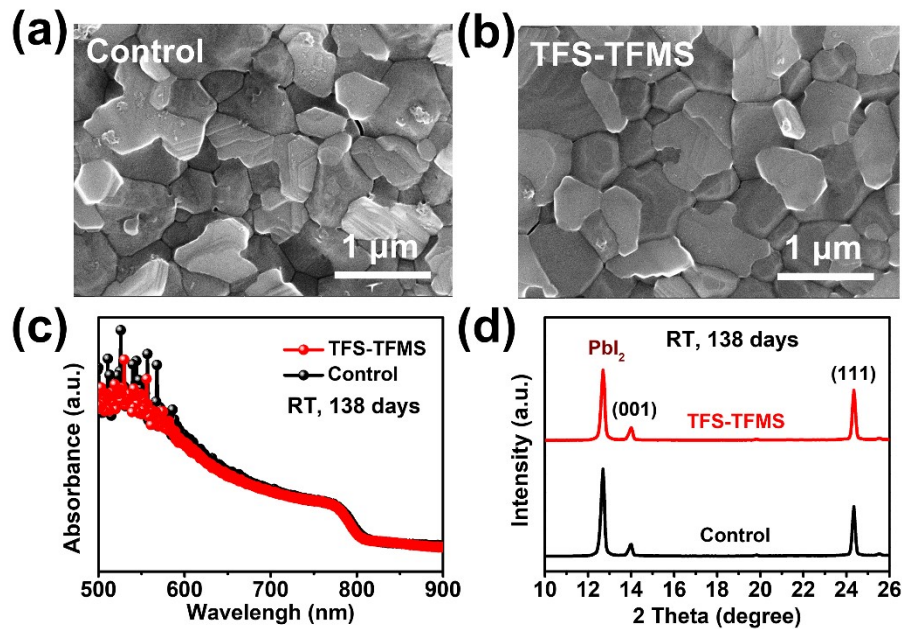


**Fig. S25** (a-b) SEM images, (c) UV-vis absorption spectra, and (d) XRD patterns of aged perovskite films without and with post-treatment *via* TFS-TFMS. The aged perovskite films were obtained by peeling off Au electrodes and washing off HTLs of PSCs. These unsealed PSCs were reserved in inert atmosphere at RT after 138 days.

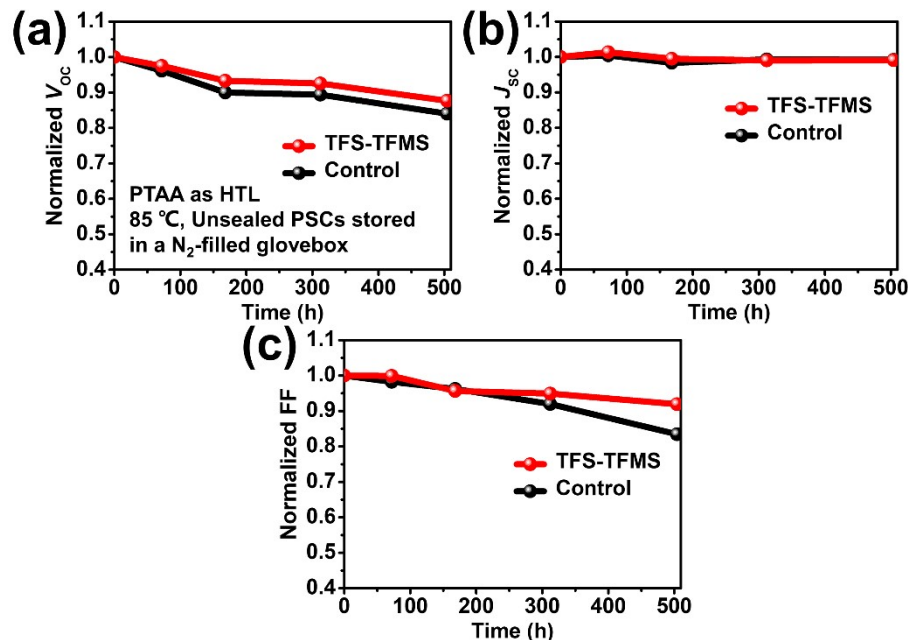


**Fig. S26** 85 °C thermal aging of the unencapsulated PSCs reserved in inert atmosphere under dark.

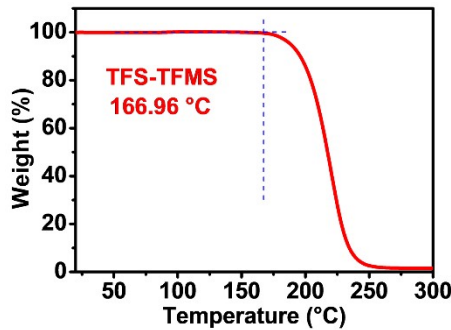


**Fig. S27** The thermogravimetric analysis (TGA) curve of TFS-TFMS powders.

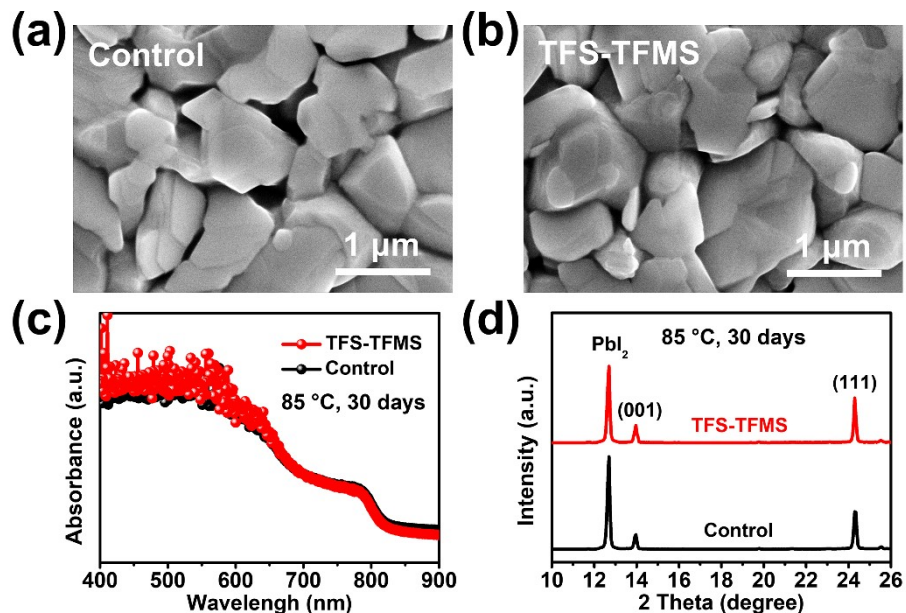


**Fig. S28** (a-b) SEM images, (c) UV-vis absorption spectra, and (d) XRD patterns of aged perovskite films without and with post-treatment *via* TFS-TFMS. These unsealed films were reserved in inert atmosphere at 85 °C under dark after 30 days.

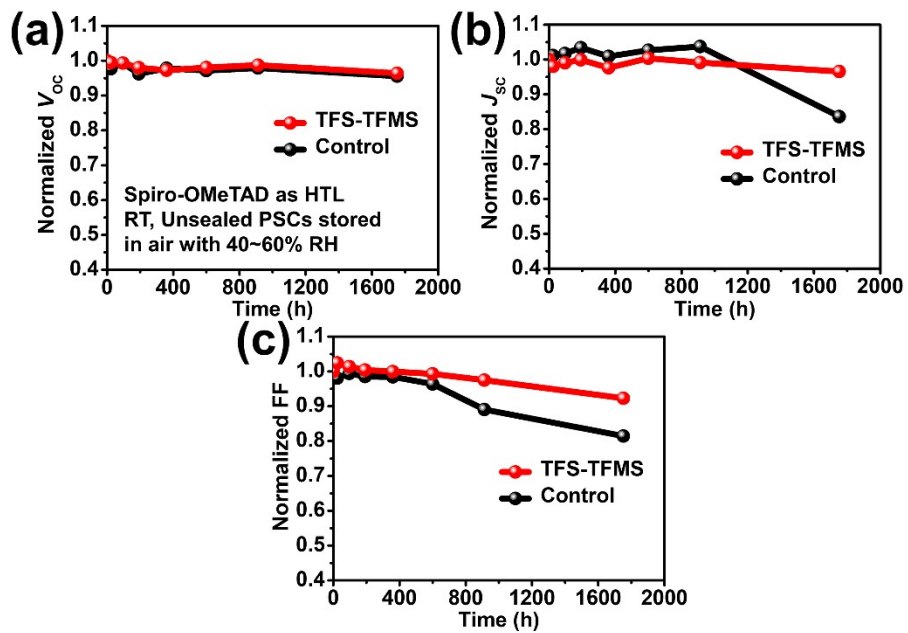


**Fig. S29** The unencapsulated PSCs were reserved in air with 40~60% RH without light illustration.

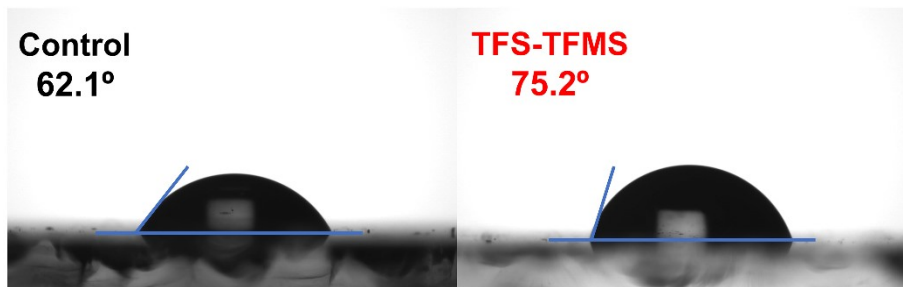


**Fig. S30** The water contact angles of the control and TFS-TFMS optimized perovskite films.

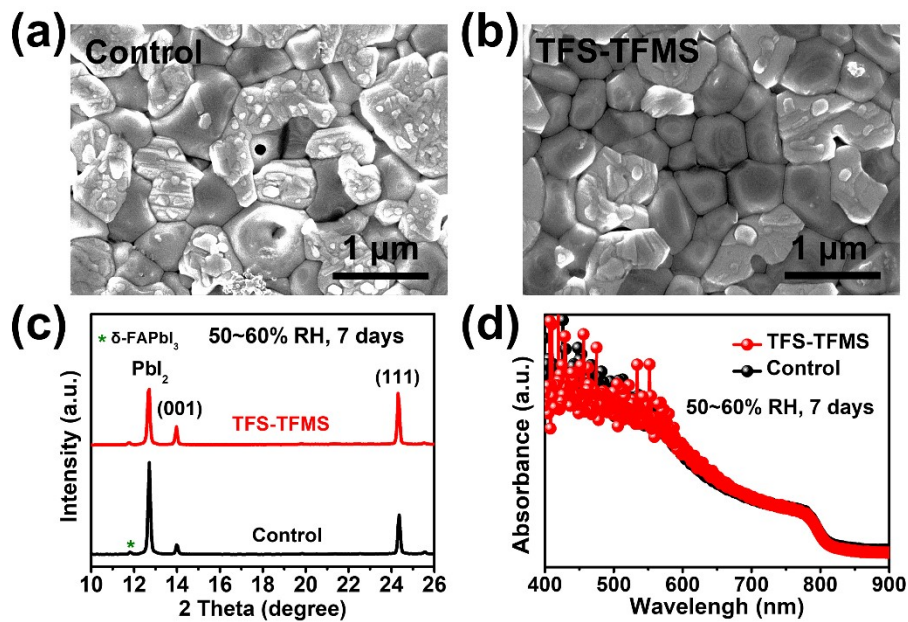


**Fig. S31** (a-b) SEM images, (c) UV-vis absorption spectra, and (d) XRD patterns of perovskite films without and with post-treatment *via* TFS-TFMS under 50~60% RH atmosphere after 7 days.

**Table S1.** The element contents from EDS mapping for the control and TFS-TFMS optimized perovskite films.

Elements	Control		TFS-TFMS	
	wt%	at%	wt%	at%
C	9.22	51.01	8.85	48.46
N	1.47	6.97	1.46	6.83
Pb	33.72	10.81	33.66	10.68
I	54.76	28.67	54.29	28.12
Cl	0.38	0.71	0.29	0.54
O	0.44	1.84	0.53	2.18
F	-	-	0.92	3.19
Total	100	100	100	100

**Table S2.** The average values of photovoltaic parameters of 20 individual PSCs using different TFS-TFMS concentrations.

TFS-TFMS (mg mL <sup>-1</sup> )	V <sub>OC</sub> (V)	J <sub>SC</sub> (mA cm <sup>-2</sup> )	FF (%)	Average PCE (%)	Best PCE (%)
0	1.108±0.007	24.47±0.21	79.36±0.77	21.57±0.23	21.99
0.5	1.121±0.007	24.37±0.21	81.40±0.66	22.24±0.21	22.60
1.0	1.129±0.007	24.50±0.20	81.74±0.75	22.60±0.19	22.93
1.5	1.138±0.007	24.66±0.20	81.30±0.78	22.83±0.33	23.56
2.0	1.129±0.005	24.35±0.18	80.93±0.69	22.26±0.25	22.80
3.0	1.123±0.010	24.27±0.23	80.56±1.12	21.95±0.43	22.63

**Table S3.** Fluorinated or sulfonate molecules passivated n-i-p PSCs.

Passivator	Chemical structure	Device structure	PCE	Year	Ref.
4-methylbenzenesulfonic acid (4-MSA)		FTO/bl-TiO <sub>2</sub> /mp-TiO <sub>2</sub> /MAPbI <sub>3</sub> @4-MSA/Spiro-OMeTAD/Au	17.58%	2017	5
pentafluoropropylammonium iodide (PFPAI)		FTO/c-TiO <sub>2</sub> /m-TiO <sub>2</sub> /Cs <sub>0.05</sub> (FA <sub>0.83</sub> MA <sub>0.17</sub> ) <sub>0.95</sub> Pb(I <sub>0.83</sub> Br <sub>0.17</sub> ) <sub>3</sub> /PFP Al/Spiro-OMeTAD/Au	16.6%	2018	6
1 <i>H</i> ,1 <i>H</i> -perfluoroctylamine (PFA)		FTO/TiO <sub>2</sub> /Cs <sub>0.05</sub> (FA <sub>0.85</sub> MA <sub>0.15</sub> ) <sub>0.95</sub> PbI <sub>2.55</sub> Br <sub>0.45</sub> /PFA/Spiro-OMeTAD/Au	21.31%	2019	7
4-(1 <i>H</i> -imidazol-3-ium-3-yl) butane-1-sulfonate (IMS)		ITO/bl-TiO <sub>2</sub> /MAPbI <sub>3</sub> @IMS/Spiro-OMeTAD/Au	20.84%	2019	8
sodium fluoride (NaF)		ITO/SnO <sub>2</sub> /(Cs <sub>0.05</sub> FA <sub>0.54</sub> MA <sub>0.41</sub> )Pb(I <sub>0.98</sub> Br <sub>0.02</sub> ) <sub>3</sub> @NaF/Spiro-OMeTAD/Au	21.92%	2019	9
guanidine sulfamate (GuaSM)		FTO/TiO <sub>2</sub> /Cs <sub>0.05</sub> (MA <sub>0.12</sub> FA <sub>0.88</sub> ) <sub>0.95</sub> Pb(I <sub>0.88</sub> Br <sub>0.12</sub> ) <sub>3</sub> @GuaSM/Spiro-OMeTAD/Au	21.66%	2020	10
sodium dodecylbenzene sulfonate (SDBS)		FTO/SnO <sub>2</sub> /MAPbI <sub>3</sub> /SDBS/Spiro-OMeTAD/Au	19.42%	2020	11
1-pyrenesulfonic acid sodium salt (PyNa <sup>+</sup> )		FTO/TiO <sub>2</sub> /PyNa <sup>+</sup> /CsFAMA-perovskite/PyNa <sup>+</sup> /Spiro-OMeTAD/Au	21.22%	2021	12
tetrafluorophthalonitrile (TFPN)		ITO/SnO <sub>2</sub> /CsFAMA-perovskite/TFPN/Spiro-OMeTAD/Ag	22.82%	2021	13
1 <i>H</i> ,1 <i>H</i> ,2 <i>H</i> ,2 <i>H</i> -perfluoroctyltriethoxysilane (PFOTES)		FTO/c-TiO <sub>2</sub> /mp-TiO <sub>2</sub> /c-SnO <sub>2</sub> /(CsPbI <sub>3</sub> ) <sub>0.1</sub> (FAPbI <sub>3</sub> ) <sub>0.875</sub> (MAPbBr <sub>3</sub> ) <sub>0.125</sub> /PFOTES/Spiro-OMeTAD/Au	20.10%	2021	14
cesium trifluoromethanesulfonate (CsCF <sub>3</sub> SO <sub>3</sub> )		FTO/SnO <sub>2</sub> /Cs <sub>0.03</sub> FA <sub>0.97</sub> PbI <sub>3</sub> /CsCF <sub>3</sub> SO <sub>3</sub> /Spiro-OMeTAD/Au	22.06%	2021	15
1,3-bis(cyanomethyl)imidazolium bis(trifluoromethyl sulfonyl)imide ([Bcim][TFSI])		FTO/cp-TiO <sub>2</sub> /mp-TiO <sub>2</sub> /(Cs <sub>0.08</sub> FA <sub>0.8</sub> MA <sub>0.12</sub> )Pb(I <sub>0.88</sub> Br <sub>0.12</sub> ) <sub>3</sub> @[Bcim][TFSI]/PEAI/Spiro-OMeTAD/Au	21.06%	2021	16
4-sulfobenzoic acid monopotassium salt (SAMS)		ITO/SnO <sub>2</sub> /Rb <sub>0.02</sub> (FA <sub>0.95</sub> Cs <sub>0.05</sub> ) <sub>0.98</sub> PbI <sub>2.91</sub> Br <sub>0.03</sub> Cl <sub>0.06</sub> @SAMS/Spiro-OMeTAD/Au	22.7%	2022	17
potassium bis(fluorosulfonyl)imide (KFSI)		ITO/SnO <sub>2</sub> /FAMA-perovskite/KFSI/Spiro-OMeTAD/Au	18.95%	2022	18

vinylaniline trifluoromethanesulfonate (VT)		FTO/ZnTiO <sub>3</sub> -ZnS/Cs <sub>0.03</sub> FA <sub>0.97</sub> PbI <sub>3</sub> /PVT/Spiro-OMeTAD/Au	24.35%	2022	19
phenylbenzimidazole sulfonic acid (PBSA)		ITO/SnO <sub>2</sub> /FA <sub>0.92</sub> MA <sub>0.08</sub> PbI <sub>3</sub> @PBSA/Spiro-OMeTAD/Au	23.27%	2022	20
3-sulfopropyl methacrylate potassium salt (SPM)		FTO/SnO <sub>2</sub> /FAPbI <sub>3</sub> @SPM/Spiro-OMeTAD/Au	21.9%	2022	21
cesium trifluoroacetate (Cs-TFA)		ITO/SnO <sub>2</sub> /FAMA-perovskite@Cs-TFA/Spiro-OMeTAD/Au	22.82%	2022	22
D-pentafluorophenylalanine (D-PFPAA)		FTO/SnO <sub>2</sub> /CsFAMA-perovskite@(D-PFPAA)/Spiro-OMeTAD/Ag	21.56%	2022	23
1-methanesulfonylpiperazine (MP)		ITO/SnO <sub>2</sub> /FAMA-Perovskite/MP/Spiro-OMeTAD/Au	23.4%	2022	24
heptadecafluoroctanesulfonic acid tetraethylammonium salt (HFSTT)		FTO/TiO <sub>2</sub> /(FAPbI <sub>3</sub> ) <sub>0.98</sub> (FAPbBr <sub>3</sub> ) <sub>0.02</sub> @HFSTT/Spiro-OMeTAD/Au	23.88%	2022	25
potassium bis(fluorosulfonyl)imide (KFSI)		ITO/SnO <sub>2</sub> /KFSI/FAMA-Perovskite/PEAI/Spiro-OMeTAD/Ag	24.17%	2023	26
poly[1-(2-acryloylethyl)-3-methylimidazolium] bis(trifluoromethane)sulfonamides (PAEMI-TFSIs)		ITO/SnO <sub>2</sub> /MAPbI <sub>3</sub> @PAEMITFSIs/Spiro-OMeTAD/MoO <sub>3</sub> /Ag	22.40%	2023	27
cobalt (II) hexafluoro-2,4-pentanedionat (CoFAC)		FTO/TiO <sub>2</sub> /FA <sub>0.90</sub> Cs <sub>0.10</sub> PbI <sub>3</sub> /CoFAC/Spiro-OMeTAD/Au	24.64%	2023	28
3,5-difluorobenzenesulfonamide (3,5-DFBS)		ITO/SnO <sub>2</sub> /FAMA-Perovskite/3,5-DFBS/Spiro-OMeTAD/Au	23.69%	2023	29
2-[N,N-bi(trifluoromethylsulfonyl)amino]pyridine (2-BTFSIP)		FTO/SnO <sub>2</sub> /FAPbI <sub>3</sub> @2-BTFSIP/Spiro-OMeTAD/Au	22.90%	2023	30
potassium 1,1,2,2,3,3-hexafluoropropene-1,3-disulfonimide (KHFDF)		ITO/SnO <sub>2</sub> /FAMA-Perovskite@KHFDF/PEAI/Spiro-OMeTAD/MoO <sub>3</sub> /Ag	24.15%	2023	31

tetra- butylammonium trifluoromethanesu- lfonate (TBASF)		ITO/SnO <sub>2</sub> /FA <sub>0.75</sub> MA <sub>0.25</sub> PbI <sub>3</sub> /TBASF/ Spiro-OMeTAD/MoO <sub>3</sub> /Ag	22.80%	2023	32
1-butyl-3- methylimidazoliu- m trifluoro- methane-sulfonate (BMIMOTF)		ITO/SnO <sub>2</sub> /(GA)(MA) <sub>5</sub> Pb <sub>5</sub> I <sub>16</sub> /BMIMO TF/Spiro-OMeTAD/Au	21.38%	2023	33
diphenyl- (trifluoromethyl)- sulfonium trifluoromethanesu- lfonate (TFS- TFMS)		ITO/SnO <sub>2</sub> /MAFAPbI <sub>3</sub> /TFS- TFMS/Spiro-OMeTAD/Au	23.56%	2024	This work

**Table S4.** Detailed photovoltaic parameters for 40 individual control PSCs.

Entry	$V_{OC}$ (V)	$J_{SC}$ (mA cm $^{-2}$ )	FF (%)	PCE (%)
1	1.104	24.54	78.31	21.23
2	1.110	24.40	80.34	21.78
3	1.107	24.48	80.31	21.78
4	1.106	24.38	79.43	21.43
5	1.107	24.67	79.62	21.76
6	1.109	24.55	79.87	21.76
7	1.115	24.28	80.47	21.79
8	1.111	24.40	79.06	21.42
9	1.118	24.07	80.32	21.61
10	1.112	24.42	79.19	21.50
11	1.102	24.47	78.16	21.06
12	1.113	24.41	80.78	21.94
13	1.113	24.12	81.24	21.80
14	1.117	24.37	79.84	21.73
15	1.111	24.40	78.39	21.25
16	1.116	24.43	79.70	21.74
17	1.103	24.35	79.78	21.43
18	1.112	24.70	79.41	21.89
19	1.117	24.54	78.56	21.63
20	1.117	24.36	78.98	21.59
21	1.108	24.54	80.53	21.99
22	1.107	24.60	79.76	21.82
23	1.112	24.35	79.14	21.51
24	1.102	24.55	79.85	21.70
25	1.110	24.77	79.09	21.83
26	1.101	24.35	78.38	21.10
27	1.104	24.26	79.87	21.48
28	1.110	24.58	80.18	21.96
29	1.105	24.68	79.88	21.87
30	1.114	24.32	79.46	21.61
31	1.110	24.40	79.12	21.52
32	1.107	24.13	79.89	21.44
33	1.108	24.55	78.65	21.48
34	1.106	24.12	78.96	21.15
35	1.097	24.40	79.55	21.38
36	1.094	24.59	78.49	21.20
37	1.091	24.81	78.98	21.46
38	1.113	24.61	78.95	21.71
39	1.107	24.78	78.45	21.62
40	1.107	24.44	78.35	21.28
Average	1.108±0.006	24.45±0.18	79.43±0.75	21.58±0.24

**Table S5.** Detailed photovoltaic parameters for 40 individual TFS-TFMS optimized PSCs.

Entry	$V_{OC}$ (V)	$J_{SC}$ (mA cm $^{-2}$ )	FF (%)	PCE (%)
1	1.142	24.81	80.27	22.76
2	1.139	24.95	80.39	22.86
3	1.137	24.76	79.81	22.47
4	1.145	24.34	80.83	22.54
5	1.148	24.65	80.30	22.72
6	1.147	24.46	82.20	23.06
7	1.143	24.12	81.14	22.38
8	1.143	24.64	80.98	22.90
9	1.138	24.90	82.15	23.38
10	1.146	24.73	82.11	23.27
11	1.126	24.63	81.16	22.60
12	1.134	24.44	80.93	22.42
13	1.132	24.76	82.34	23.18
14	1.135	24.99	81.93	23.35
15	1.138	24.95	80.84	22.96
16	1.134	24.72	80.95	22.78
17	1.139	24.45	81.84	22.79
18	1.133	24.62	81.17	22.64
19	1.134	24.81	82.36	23.17
20	1.133	24.77	81.35	22.84
21	1.123	24.62	81.07	22.40
22	1.126	24.47	81.52	22.55
23	1.138	24.73	82.61	23.34
24	1.138	24.80	83.10	23.56
25	1.135	24.92	80.99	22.99
26	1.128	24.72	81.49	22.81
27	1.125	24.57	83.14	23.00
28	1.141	24.60	82.15	23.07
29	1.139	24.94	82.39	23.40
30	1.141	24.70	81.41	22.94
31	1.144	25.01	80.77	23.10
32	1.143	24.89	80.77	22.98
33	1.135	24.47	82.48	22.91
34	1.138	24.40	81.83	22.72
35	1.118	24.65	82.59	22.79
36	1.126	24.49	81.23	22.40
37	1.131	24.16	81.82	22.36
38	1.126	24.42	81.29	22.38
39	1.112	24.63	81.92	22.39
40	1.137	24.57	80.73	22.56
Average	1.135±0.008	24.66±0.21	81.51±0.79	22.84±0.33

**Table S6.** Photovoltaic parameters of the control and TFS-TFMS optimized PSCs under forward (FS) and reverse (RS) scan directions.

Devices	Scan direction	$V_{OC}$ (V)	$J_{SC}$ (mA cm $^{-2}$ )	FF (%)	PCE (%)	HI (%)*)
Control	RS	1.108	24.54	80.53	21.99	7.91
	FS	1.082	24.61	76.04	20.25	
TFS-TFMS	RS	1.138	24.80	83.10	23.56	4.58
	FS	1.124	24.95	80.16	22.48	

\*Note: Hysteresis index (HI) = (PCE<sub>RS</sub> - PCE<sub>FS</sub>) / PCE<sub>RS</sub>

**Table S7.** EIS parameters of the control and TFS-TFMS optimized devices without applying bias voltages under dark.

Devices	$R_{tr}$ ( $\Omega$ )	CPE1 (F)	$R_{rec}$ ( $\Omega$ )	CPE2 (F)
Control	37805	7.68E-09	7.30E+05	8.59E-07
TFS-TFMS	25885	9.59E-09	8.26E+05	1.08E-06

## References

1. R. H. Yuan, B. Cai, Y. H. Lv, X. Gao, J. W. Gu, Z. H. Fan, X. H. Liu, C. Yang, M. Z. Liu and W. H. Zhang, *Energy Environ. Sci.*, 2021, **14**, 5074-5083.
2. B. Delley, *J. Chem. Phys.*, 1990, **92**, 508-517.
3. B. Delley, *J. Chem. Phys.*, 2000, **113**, 7756-7764.
4. S. J. Clark, M. D. Segall, C. J. Pickard, P. J. Hasnip, M. I. J. Probert, K. Refson and M. C. Payne, *Kristallogr.*, 2005, **220**, 567-570.
5. F. Han, J. S. Luo, H. A. Malik, B. W. Zhao, Z. Q. Wan and C. Y. Jia, *J. Power Sources*, 2017, **359**, 577-584.
6. K. M. M. Salim, T. M. Koh, D. Bahulayan, P. C. Harikesh, N. F. Jamaludin, B. Febriansyah, A. Bruno, S. Mhaisalkar and N. Mathews, *ACS Energy Lett.*, 2018, **3**, 1068-1076.
7. P. F. Guo, Q. Ye, X. K. Yang, J. Zhang, F. Xu, D. Shchukin, B. Q. Wei and H. Q. Wang, *J. Mater. Chem. A*, 2019, **7**, 2497-2506.
8. W. R. Zhou, D. Li, Z. G. Xiao, Z. L. Wen, M. M. Zhang, W. P. Hu, X. J. Wu, M. T. Wang, W. H. Zhang, Y. L. Lu, S. H. Yang and S. F. Yang, *Adv. Funct. Mater.*, 2019, **29**, 1901026.
9. N. X. Li, S. X. Tao, Y. H. Chen, X. X. Niu, C. K. Onwudinanti, C. Hu, Z. W. Qiu, Z. Q. Xu, G. H. J. Zheng, L. G. Wang, Y. Zhang, L. Li, H. F. Liu, Y. Z. Lun, J. W. Hong, X. Y. Wang, Y. Q. Liu, H. P. Xie, Y. L. Gao, Y. Bai, S. H. Yang, G. Brocks, Q. Chen and H. P. Zhou, *Nat. Energy*, 2019, **4**, 408-415.
10. X. P. Liu, J. H. Wu, Y. Q. Yang, D. Wang, G. D. Li, X. B. Wang, W. H. Sun, Y. L. Wei, Y. F. Huang, M. L. Huang, L. Q. Fan, Z. Lan, J. M. Lin and K. C. Ho, *Small*, 2020, **16**, 2004877.
11. Y. Q. Zou, R. J. Guo, A. Buyruk, W. Chen, T. X. Xiao, S. S. Yin, X. Y. Jiang, L. P. Kreuzer, C. Mu, T. Ameri, M. Schwartzkopf, S. V. Roth and P. Müller-Buschbaum, *ACS Appl. Mater. Interfaces*, 2020, **12**, 52643-52651.
12. L. L. Gao, H. Su, Z. Xu, Y. J. Hu, J. Zhang and S. Z. Liu, *Sol. RRL*, 2021, **5**, 2100416.
13. X. L. Gong, H. M. Li, R. N. Zhou, X. Peng, Y. K. Ouyang, H. X. Luo, X. C. Liu, J. Zhuang, H. Y. Wang, Y. F. Ni and Y. Lei, *ACS Appl. Mater. Interfaces*, 2021, **13**, 41149-41158.
14. H. Kanda, O. J. Usiobo, C. Momblona, M. Abuhelaiqa, A. A. Sutanto, C. Igci, X. X. Gao, J. N. Audinot, T. Wirtz and M. K. Nazeeruddin, *Sol. RRL*, 2021, **5**, 2000650.
15. R. H. Chen, Y. K. Wang, S. Q. Nie, H. Shen, Y. Hui, J. Peng, B. H. Wu, J. Yin, J. Li and N. F. Zheng, *J. Am. Chem. Soc.*, 2021, **143**, 10624-10632.
16. X. X. Gao, B. Ding, H. Kanda, Z. F. Fei, W. Luo, Y. Zhang, N. Shibayama, A. Züttel, F. F. Tirani, R. Scopelliti, S. Kinge, B. Zhang, Y. Q. Feng, P. J. Dyson and M. K. Nazeeruddin, *Cell Rep. Phys. Sci.*, 2021, **2**, 100475.
17. L. Bai, F. Yao, R. Wang, B. B. Liu, D. M. He, Q. Zhou, W. Q. Wang, C. Y. Xu, X. B. Hu, S. Q. Chen, Q. L. Song, T. W. Zhou, D. Lee, P. J. Zhao, C. Chen, H. Yang, Q. Q. Lin, Z. G. Zang and J. Z. Chen, *Sci. China-Mater.*, 2022, **65**, 3368-3381.
18. Q. Chen, G. M. Zhai, J. T. Ren, Y. Huo, Z. K. Yun, H. L. Jia, Y. W. Gao, C. Y. Yu and B. S. Xu, *Org. Electron.*, 2022, **107**, 106544.
19. Q. F. Feng, X. F. Huang, Z. H. Tang, Y. L. Hou, Q. Chang, S. Q. Nie, F. Cao, X. Y. Niu, J. Yin, J. Li, N. F. Zheng and B. H. Wu, *Energy Environ. Sci.*, 2022, **15**, 4404-4413.
20. Y. Q. Hu, Z. Y. He, X. R. Jia, S. F. Zhang, Y. F. Tang, J. Wang, M. M. Wang, G. P. Sun, G. L. Yuan and L. Y. Han, *Small Methods*, 2022, **6**, 2101257.

21. Z. D. Liu, C. H. Duan, F. Liu, C. C. S. Chan, H. P. Zhu, L. G. Yuan, J. Li, M. J. Li, B. Zhou, K. S. Wong and K. Y. Yan, *Small*, 2022, **18**, 2105196.
22. F. Z. Qiu, J. Y. Sun, H. Liu and J. J. Qi, *Chem. Eng. J.*, 2022, **446**, 136936.
23. H. Y. Wang, W. J. Zou, Y. K. Ouyang, X. Deng, H. Luo, J. H. Xu, X. C. Liu, H. M. Li, X. L. Gong, Y. Lei, Y. F. Ni and Y. S. Peng, *J. Mater. Chem. A*, 2022, **10**, 10750-10758.
24. X. Yu, Y. H. Lv, B. Y. Xue, L. Wang, W. P. Hu, X. H. Liu, S. F. Yang and W. H. Zhang, *Nano Energy*, 2022, **93**, 106856.
25. J. Zhu, Y. T. Qian, Z. J. Li, O. Y. Gong, Z. F. An, Q. Liu, J. H. Choi, H. Guo, P. J. Yoo, D. H. Kim, T. K. Ahn, G. S. Han and H. S. Jung, *Adv. Energy Mater.*, 2022, **12**, 2200632.
26. C. Gong, C. Zhang, Q. X. Zhuang, H. Y. Li, H. Yang, J. Z. Chen and Z. G. Zang, *Nano-Micro Lett.*, 2023, **15**, 17.
27. N. C. Guan, G. Wu, J. Wang, Y. Q. Bao, W. Hui, Z. Q. Deng, L. Gu, X. Y. Gao, J. Zhang, P. Müller-Buschbaum and L. Song, *ACS Appl. Mater. Interfaces*, 2023, **15**, 26872-26881.
28. Z. J. Li, M. Z. Wu, L. Yang, K. P. Guo, Y. W. Duan, Y. Li, K. He, Y. F. Xing, Z. Zhang, H. Zhou, D. F. Xu, J. G. Wang, H. Zou, D. Li and Z. K. Liu, *Adv. Funct. Mater.*, 2023, **33**, 2212606.
29. Y. Liu, H. P. Zhou, J. X. Song, W. Y. Wang and H. Q. Wang, *Sol. RRL*, 2023, **7**, 2300028.
30. C. M. Tian, Y. Zhao, X. F. Han, B. Li, Y. C. Rui, H. Xiong, Y. Qiu, W. An, K. R. Li, C. Y. Hou, Y. G. Li, H. Z. Wang and Q. H. Zhang, *Chem. Eng. J.*, 2023, **452**, 139345.
31. X. B. Yuan, R. Li, Z. Xiong, P. Y. Li, G. O. Odunmbaku, K. Sun, Y. H. Deng and S. J. Chen, *Adv. Funct. Mater.*, 2023, **33**, 2215096.
32. Z. L. Zhang, Z. X. Jiang, W. X. Ji, J. F. Fu, T. Wu, W. T. Wu, D. Rui, P. Xu, Y. Zhou, B. Dong and B. Song, *Adv. Energy Sustainability Res.*, 2023, **4**, 2200173.
33. H. L. Zheng, X. F. Peng, T. X. Chen, T. Zhang, S. H. Yuan, L. Wang, F. Qian, J. Huang, X. D. Liu, Z. D. Chen, Y. N. Zhang and S. B. Li, *J. Energy Chem.*, 2023, **84**, 354-362.